Calculation of Multiplicity of Steady States in a Catalyst Pellet by Homotopic Continuation Method

Pablo Giunta, Norma Amadeo, Miguel Laborde, and María Bergamini
Laboratorio de Procesos Catalíticos, Dpto Ingeniería Química, Facultad de Ingeniería, Universidad de Buenos Aires, Argentina

DOI 10.1002/aic.12267
Published online April 28, 2010 in Wiley Online Library (wileyonlinelibrary.com).

Many exothermic reactions, such as the oxidation of CO in a catalyst pellet may present multiplicity of steady states. Experimental results suggest this behavior in a copper ceria catalyst, and this in turn would indicate that the kinetics should be nonmonotonic with respect to reactants' compositions. The model for the reaction is described by a two-point boundary value problem that is hard to solve with direct methods, even when seeking a single solution. The aim of this work is to implement a homotopic method to find all the steady states of this kind of problems. The search for solutions is driven by a pseudo arclength continuation. Homotopic curves that passes through all possible solutions are obtained. Also, a study of the dependence of the initial point upon the curve is performed. © 2010 American Institute of Chemical Engineers *AIChE J,* 57: 473–481, 2011

Keywords: homotopy, CO oxidation, multiplicity, nonmonotonic kinetics

Introduction

Steady states multiplicity in chemical engineering takes place when some feedback process (e.g., diffusion, heat conduction or counter-current contact) occurs, in addition to a nonmonotonic behavior of the reaction rate with respect to composition or temperature.[1] These two conditions must occur simultaneously. Thus, multiplicity shall not be observed, for instance, in a single phase plug flow reactor or an isothermal pellet with a simple power-law kinetics of the form kc_A^n.

The nonmonotonic behavior could be because of:

(a) Thermal effects: When dealing with an exothermic reaction, temperature rises as reactants depletion advances; the nonmonotonic effect lies on the fact that temperature tends to increase the rate of reaction, whereas reactants depletion has the opposite effect.

(b) Concentration effects: This situation happens in catalysis when reactants compete for the same active site, thus obtaining a nonmonotonic kinetics (e.g., Langmuir); besides this nonmonotonicity, the dependence must be sharp enough.

The steady state multiplicity was first studied about 50 years ago, in the work of Bilous and Amundson.[2] Then, Aris and Amundson[3–5] developed a systematic analysis of the dynamic behavior of CRST, where an exothermic reaction takes place. Jorgensen et al.[6] extended these studies to a reaction system in series. Moreover, Balakotaiah and Luss[7] applied catastrophe theory to analyze the influence of residence time and temperature in a CRST where more than one reaction takes place simultaneously. On the other hand, Lee et al.[8] examined steady states multiplicity in a plug flow tubular reactor with axial dispersion and nonuniform catalyst activity.

Numerous works studied the porous catalyst pellet dynamics. The existence of multiple steady states in a catalyst

Correspondence concerning this article should be addressed to M. Bergamini at lbergamini@fi.uba.ar.

pellet was proved by Weisz and Hicks[9] and by Amundson and Raymond.[10] Further, Van den Bosch and Luss[11] studied multiplicity and uniqueness criteria for positive-order reactions; Hu et al.[12,13] analyzed the dependence of the multiplicity on the order of reaction and the geometry in a catalyst pellet. Besides, Nielsen and Villadsen[14] considered the dynamic behavior in a catalyst pellet when diffusion, reaction, and absorption take place simultaneously, and they found that up to five steady states may occur. Likewise, Tsotsis[15] and Schmitz and Tsotsis[16] studied the dynamic behavior in catalysts. They analyzed the instabilities in catalyst systems for both exothermic and endothermic reactions.

More recently, Botero et al.[17] proved the existence of multiplicity and dynamic bifurcation phenomena in an enzymatic process, where diffusion and reaction occur simultaneously.

This work arises from experimental evidence observed in the CO oxidation reaction, using a Cu/CeO_2 catalyst. In a lab-scale reactor, working in the absence of diffusion effects, a decrease of the reaction rate was observed, when the catalyst pellet size decreased. This fact induces to study diffusion-reaction phenomena inside the pellet with a mathematical model. The model allows predicting that for certain pellet sizes not only the reaction rate (or more precisely, the effectiveness factor) increases but also steady state multiplicity takes place. Experimental results are shown in Table 1.[18]

The aim of this work is to analyze the multiplicity of steady states in a catalyst pellet where the CO oxidation reaction occurs, using a mathematical model. The diffusion-reaction problem is associated to a two-point boundary value problem. If multiplicity occurs, the nonlinear mathematical model generated has more than one solution. Therefore, a homotopy continuation method, adapted to find all of the solutions of two-point boundary value problems, was used.

Homotopy continuation methods have the advantage of reaching the solution by tracing a path from a fairly arbitrary initial point.[19] It is a global method that can calculate all solutions in a nonlinear model. Examples of homotopy continuation to find all solutions of algebraic nonlinear systems of equations can be found in chemical engineering literature.[19,20]

The beginning of the practical use of homotopy methods in solving system of equations is attributed to Davidenko,[21] and this topic has received contributions by several researchers.[22–26] Allgower and Georg[26] played an essential role in popularizing the method.

The homotopy continuation method was widely used to calculate all solutions of a system of algebraic equations $\underline{F}(\underline{\theta}) = \underline{0}$, with $\underline{\theta} \in R^{Nn}$ and $\underline{F} : D \subset R^{Nn} \rightarrow R^{Nn}$. A homotopy function is defined with a homotopy parameter t, $\underline{H}(\underline{\theta}; t) = \underline{0}$, $\underline{H}: D \times R \subset R^{Nn+1} \rightarrow R^{Nn}$, such that $\underline{H}(\underline{\theta}; 0) = \underline{G}(\underline{\theta})$ and $\underline{H}(\underline{\theta}; 1) = \underline{F}(\underline{\theta})$, where $\underline{G}(\underline{\theta})$ is an "easy" function. The idea is to numerically follow the path determined by the equation $\underline{H}(\underline{\theta}; t) = \underline{0}$ in $D \times R$.

In this work, the capabilities of the homotopy method of finding all solutions, which are generally used in algebraic systems, are exploited to handle the BVP problem.

Problem Statement

This work deals with a catalyst pellet of slab geometry ($a = 1$) in which an exothermic reaction takes place. The following hypotheses were considered to simplify the model:

Table 1. CO Conversion for Different Temperatures and Pellet Sizes

T (K)	R_p < 4.4 μm	4.4 μm < R_p < 6.2 μm	6.2 μm < R_p < 8.8 μm
423	0.48	0.60	0.68
443	0.60	0.72	0.86
463	0.71	0.85	0.95

- Negligible pressure drop inside the pellet.
- Constant thermodynamic properties (heat capacity and reaction enthalpy).
- Constant thermal conductivity.
- Dusty Gas Model (DGM) for mass flow.[27,28]
- No external film effects, i.e. Sh, Nu $\rightarrow \infty$.
- Unidimensional problem.

When these hypotheses hold the problem can be described by the following model[29]

$$\frac{dp_j}{dz} = R_p RT \sum_k B_{jk} N_k \tag{1}$$

$$\frac{dT}{dz} = R_p \frac{q}{\kappa} \tag{2}$$

$$\frac{dN_j}{dz} = \begin{cases} -R_p \sum_i \alpha_{ij} r_i + \frac{a-1}{1-z} N_j & z \neq 1 \\ -\frac{1}{a} R_p \sum_i \alpha_{ij} r_i & z = 1 \end{cases} \tag{3}$$

$$\frac{dq}{dz} = \begin{cases} -\sum_k C_{p_k} N_k \frac{dT}{dz} + R_p \sum_i \Delta H_i r_i + \frac{a-1}{1-z} q & z \neq 1 \\ \frac{1}{a} R_p \sum_i \Delta H_i r_i & z = 1 \end{cases} \tag{4}$$

$$\begin{array}{ll} p_j = p_j^{\sup}, T = T^{\sup} & z = 0 \\ N_j = 0, q = 0 & z = 1 \end{array} \tag{5}$$

where $z = 0$ is the catalyst surface and $z = 1$ is the catalyst center. The definition of the DGM matrix B can be found in Krishna et al.[27,28,30] Equations 1–4 can be rewritten in matrix notation

$$\frac{d\underline{p}}{dz} = R_p R\, T\, \underline{\underline{B}} \cdot \underline{N} \tag{6}$$

$$\frac{dT}{dz} = R_p \frac{q}{\kappa} \tag{7}$$

$$\frac{d\underline{N}}{dz} = \begin{cases} -R_p \underline{r} \cdot \underline{\underline{\alpha}} + \frac{a-1}{1-z} \underline{N} & z \neq 1 \\ -\frac{1}{a} R_p \underline{r} \cdot \underline{\underline{\alpha}} & z = 1 \end{cases} \tag{8}$$

$$\frac{dq}{dz} = \begin{cases} -\underline{C}_p^T \cdot \underline{N} \frac{dT}{dz} + Rp\ \underline{r} \cdot \Delta \underline{H} + \frac{a-1}{1-z} q & z \neq 1 \\ \frac{1}{a} R_p\ \underline{r} \cdot \Delta \underline{H} & z = 1 \end{cases} \tag{9}$$

After solving this system, the effectiveness factor is calculated by

$$\eta_j = \frac{a}{R_p} \frac{N_j^{\sup}}{r_j^{\sup}} \tag{10}$$

The system so defined represents mathematically a boundary value problem with essential conditions on $z = 0$ (partial pressures and temperature) and natural conditions on $z = 1$ (mass and energy fluxes). Next section deals with this issue.

Homotopy Continuation Method

Homotopy function

The problem to solve is a two-point boundary value problem. The goal is to find all solutions of the problem, that is, all steady states of the system. It is known that usual methods for solving this kind of problems (collocation, discretization, shooting, etc.) can find only one solution at a time. Moreover, all these methods will eventually lead to a nonlinear system of equations, which has to be solved with an iterative method. Therefore, initial values close to the solution are required to converge. If all solutions are sought, a large set of initial values over the entire feasible domain should be tried.

The homotopy method can find all solutions of a system of algebraic equations in a fairly automatic way, and (almost) no care should be taken in selecting a good initial point. As it was mentioned in the Introduction, the method consists on tracing a curve described by the zeros of an homotopy function $\underline{H}(\underline{\theta};t) = \underline{0}$. For $t = 0$, all solutions of $\underline{H}(\underline{\theta};0) = \underline{0}$ are known, and when $t = 1$, $\underline{H}(\underline{\theta};1) = \underline{0}$ coincides with the original problem whose solutions are sought.

To use homotopy continuation in our problem, the BVP is transformed into an algebraic equation. By means of the shooting method, the BVP may be solved as a zero-finding problem. Watson[31] describes a homotopy-type algorithm for certain BVP problems and proves that under certain hypotheses, it converges to a solution for almost all initial point within a bounded set.

In this work, the pseudo arclength algorithm is used to follow the homotopy curve defined by $\underline{H}(\underline{\theta};t) = \underline{0}$. As all solutions of the problem are sought, the homotopy parameter t shall not be limited to be in the interval [0,1], but we let it go beyond these limits. In that way, the homotopy curve may cross several times the level $t = 1$, passing by several solutions of the problem.

Following Hlavacek,[32] the problem of finding steady states of a reaction in a catalyst pellet can be stated as follows: a vectorial function $\underline{F}$: $R^{\mathrm{Nn}} \rightarrow R^{\mathrm{Nn}}$, which represents the boundary conditions in $z = 1$, that is, mass and heat fluxes at the center of the pellet calculated with a trial value $\underline{\theta}$ of the fluxes in $z = 0$.

$$\underline{F}(\underline{\theta}) = \begin{bmatrix} \underline{N}(\underline{\theta}, z=1) \\ \underline{q}(\underline{\theta}, z=1) \end{bmatrix}^{\mathrm{calc}} \tag{11}$$

where $\underline{\theta}$ is conveniently scaled and made dimensionless, $\theta_1 = \frac{N_{\mathrm{co}}}{10^4 \mathrm{mol\,m^{-2}\,s^{-1}}}$ and $\theta_2 = \frac{q}{10^{-9} \mathrm{J\,m^{-2}\,s^{-1}}}$. In this way, both elements of $\underline{\theta}$ are in a similar order of magnitude (about 10^0–10^1). For each value of $\underline{\theta}$, $\underline{F}$ can be computed by a numerical integration. A solution of the problem is such that mass and heat fluxes at the center of the pellet are zero, that is, $\underline{F} = \underline{0}$. Then, the solution procedure is constituted by two steps: integration and zero-finding schemes.

The zeros of $\underline{F}$ may be obtained by means of Newton's method

$$\underline{\theta}^{(r+1)} = \underline{\theta}^{(r)} - \underline{\underline{F}}_{\theta}^{-1}\left(\underline{\theta}^{(r)}\right) \cdot \underline{F}\left(\underline{\theta}^{(r)}\right) \tag{12}$$

performing the integration in each step. A drawback of this method, as it is well known, is that the initial trial value must be close to the real value and it can find only one solution at the most. To overcome this problem, a continuation method consisting on embedding the function $\underline{F}$ in a homotopy function $\underline{H}$: $R^{\mathrm{Nn}+1} \rightarrow R^{\mathrm{Nn}}$ is used. In general, the function $\underline{H}$ has the form

$$\underline{H}(\underline{\theta};t) = t\,\underline{F}(\underline{\theta}) + (1-t)\underline{G}(\underline{\theta}) \tag{13}$$

where t is a new parameter in the problem called homotopy parameter. It must be said that in this work the homotopy parameter t has no physical meaning but the method needs it to guide the homotopy curve towards the physical solutions. Clearly, a vector value $\underline{\theta}_0$ such that $\underline{H}(\underline{\theta}_0;0) = \underline{0}$ is a root of $\underline{G}$, whereas a vector value $\underline{\theta}^*$ such that $\underline{H}(\underline{\theta}^*;1) = \underline{0}$ is a root of $\underline{F}$.

Under certain differentiability conditions on $\underline{F}$ and $\underline{G}$,[24,33] the Implicit Function Theorem shows that the set of points $(\underline{\theta},t)$ in $R^{\mathrm{Nn}+1}$, such that $\underline{H}(\underline{\theta};t) = \underline{0}$ is a smooth one-dimensional curve.

The key idea of the method is to trace numerically the solution curve of $\underline{H}(\underline{\theta};t) = \underline{0}$ from $(\underline{\theta}_0;0)$. The function $\underline{G}$ is chosen so that the solution of $\underline{G}(\underline{\theta}) = \underline{0}$ is easy to compute. Two of the possible choices for this function are $\underline{G}(\underline{\theta}) = \underline{\theta} - \underline{\theta}_0$ (fixed point homotopy) or $\underline{G}(\underline{\theta}) = \underline{F}(\underline{\theta}) - \underline{F}(\underline{\theta}_0)$ (Newton homotopy), for a proper value $\underline{\theta}_0$.

In this work, the "easy" function $\underline{G}$ chosen was $\underline{\theta} - \underline{\theta}_0$. $\underline{\theta}_0$ is the initial value (at $t = 0$), and remains unchanged along the curve. The elements of both $\underline{F}$ and $\underline{G}$ are conveniently scaled, as their values are very different in order of magnitude.

The simplest way to trace the zero-curve is using a predictor-corrector method,[26] parametrizing the with t, that is,

$$\underline{H}(\underline{\theta}(t);t) = \underline{0} \tag{14}$$

Given a point $(\underline{\theta}_u;t_u)$ on the curve, and the tangent vector $\frac{d\underline{\theta}_u}{dt}$, a new point in the curve for $t_{u+1} = t_u + \Delta t_u$ is approximated in the predictor step by

$$\underline{\theta}_{u+1}^{(0)} = \underline{\theta}_u + \frac{d\underline{\theta}_u}{dt}\Delta t_u \tag{15}$$

and then corrected back to the curve $\underline{H} = \underline{0}$ using the point $(\underline{\theta}_{u+1}^{(0)};t_{u+1})$ as the initial guess for the corrector step. The correction is made by means of Newton's method,

$$\underline{\underline{H}}_{\theta}\left(\theta_{u+1}^{(r)};t_{u+1}\right) \cdot \Delta\underline{\theta}_{u+1}^{(r)} = -\underline{H}\left(\theta_{u+1}^{(r)};t_{u+1}\right) \tag{16}$$

Once the method converge, the last value of $\Delta\theta_{u+1}$ is used to compute the next point on the curve

$$\underline{\theta}_{u+1} = \underline{\theta}_u + \Delta\underline{\theta}_{u+1} \tag{17}$$

If $\underline{\underline{H}}_{\theta}(\underline{\theta}_{u+1};t_{u+1})$ is nonsingular, the Newton iterations converge for a sufficiently small Δt_u. Finally, the new tangent vector can be calculated with

$$\underline{\underline{H}}_{\theta}\left(\underline{\theta}_{u+1};t_{u+1}\right)\cdot\frac{d\underline{\theta}_{u+1}}{dt}=-\underline{H}_{t}\left(\underline{\theta}_{u+1};t_{u+1}\right) \tag{18}$$

Equation 18 is obtained differentiating Eq. 14 w.r.t. t.

When multiplicity occurs, there may be more than one $\underline{\theta}$ at $t=1$ that makes $\underline{H}=\underline{0}$, namely, the zero curve crosses $t=1$ more than once. This is possible if

(a) The curve turns backwards after crossing $t=1$.

(b) The curve bifurcates.

When case (a) occurs, the point in which the curve turns is called turning point. Let $\underline{X}=\begin{bmatrix}\underline{\theta}\\ t\end{bmatrix}$. Mathematically, turning points arise in points where $rank(\underline{\underline{H}}_{\underline{X}})=Nn$ and $rank(\underline{\underline{H}}_{\theta})=Nn-1$. That is, the null space of $\underline{\underline{H}}_{\theta}$ has dimension 1 and $\underline{H}_t$ does not belong to its range. Therefore, $\underline{H}_t$ has to be zero in Eq. 18 and $\frac{d\underline{\theta}}{dt}$, if nonzero generates the null space of $\underline{\underline{H}}_{\theta}$. The important point is that $\underline{\underline{H}}_{\theta}$ is singular and the Newton's iterations, Eqs. 15–17 fails to converge.

Case (b) occurs when $rank(\underline{\underline{H}}_{\theta})=Nn-2$ and $\underline{H}_t\notin \text{range}(\underline{\underline{H}}_{\theta})$ or when $rank(\underline{\underline{H}}_{\theta})=\text{Nn}-1$ and $\underline{H}_t\in\text{range}(\underline{\underline{H}}_{\theta})$. In both cases, there are two directions to follow in the curve. In the problem presented here, no bifurcation was detected.

In both cases, the simple tracking-curve method described above, Eqs. 15–18 fails as it implies calculating a unique solution for each value of t that increases monotonically. Then, as proposed by Keller,[34] the zero-curve of $\underline{H}$ is calculated by a pseudo arclength homotopy.

Pseudo arclength homotopy continuation

To trace the curve beyond turning and bifurcation points, both t and $\underline{\theta}$ are reparametrized with the arclength s. By definition of the arclength

$$\|\dot{\underline{\theta}}\|^2+(\dot{t})^2=1 \tag{19}$$

where $\dot{\underline{\theta}}=\frac{d\underline{\theta}}{ds}$ and $\dot{t}=\frac{dt}{ds}$. Equation 19 can be approximated and rearranged in the following form[35]

$$\Delta s\approx\Delta\underline{\theta}^T\cdot\dot{\underline{\theta}}+\Delta t\,\dot{t} \tag{20}$$

The Keller's pseudo arclength method traces the zero-curve of the function $\underline{\varepsilon}:R^{\text{Nn}+1}\rightarrow R^{\text{Nn}+1}$, defined as

$$\underline{\varepsilon}(\underline{X})=\begin{bmatrix}\underline{H}\\ \varphi\end{bmatrix} \tag{21}$$

. The new function added is

$$\varphi=\left(\underline{\theta}-\underline{\theta}^{(0)}\right)^T\cdot\dot{\underline{\theta}}+\left(t-t^{(0)}\right)\dot{t}-\Delta s \tag{22}$$

where $\underline{\theta}^{(0)}$ and $t^{(0)}$ are reasonable starting values of the corrector step.

If $\underline{X}^0$ is such that $\underline{\varepsilon}(\underline{X}^0)=\underline{0}$ and $rank(\underline{\underline{\varepsilon}}_{\underline{X}}(\underline{X}^0))=Nn$, the implicit function theorem states that there exist a unique zero-curve of Eq. 21 through $\underline{X}^0$, which is called solution branch.

Note that

$$\underline{\underline{\varepsilon}}_{\underline{X}}=\begin{bmatrix}\underline{\underline{H}}_{\theta} & \underline{H}_t\\ \dot{\underline{\theta}} & \dot{t}\end{bmatrix} \tag{23}$$

from what it is clear that $\underline{\underline{\varepsilon}}_{\underline{X}}$ is nonsingular in turning points, even when $\underline{\underline{H}}_{\theta}$ is singular.

The Newton's method is applied to $\underline{\varepsilon}$, to find the root $\underline{X}$ with

$$\underline{X}^{(r+1)}=\underline{X}^{(r)}-\underline{\underline{\varepsilon}}_{\underline{X}}^{-1}\left(\underline{X}^{(r)}\right)\cdot\underline{\varepsilon}\left(\underline{X}^{(r)}\right) \tag{24}$$

Iterations stop when $\left\|\underline{X}^{(r+1)}-\underline{X}^{(r)}\right\|<$tol, for a given tolerance. Each point in the curve is calculated iteratively by Eq. 24.

Partial derivatives of $\underline{H}$ and φ are needed to obtain $\underline{\underline{\varepsilon}}_{\underline{X}}$. Like $\underline{F}$ in Eq. 11, $\underline{\underline{H}}_{\theta}$ in Eq. 23 must somehow be the result of the integration inside the catalyst pellet. Therefore, the corresponding differential equations must be found. Some new variables are defined by

$$\begin{cases}\pi_{nj}=\frac{\partial p_j}{\partial\theta_n};\tau_n=\frac{\partial T}{\partial\theta_n}\\ \nu_{nj}=\frac{\partial N_j}{\partial\theta_n};\lambda_n=\frac{\partial q}{\partial\theta_n}\end{cases}$$

where $\underline{\underline{\pi}}=\underline{\underline{p}}_{\theta}$, $\underline{\tau}=\underline{T}_{\theta}$, $\underline{\underline{\nu}}=\underline{\underline{N}}_{\theta}$, $\underline{\lambda}=\underline{q}_{\theta}$. It will also be convenient to introduce the variables $\underline{\xi}=\begin{bmatrix}p\\ \overline{T}\end{bmatrix}$ and $\underline{\underline{\psi}}=[\underline{\underline{\pi}}\quad\underline{\tau}]$.

From Eqs. 1–5 the differential equations to be solved together with Eqs. 6–9 are (see Appendix A)

$$\frac{d\underline{\underline{\pi}}}{dz}=R_pR\left[\underline{\tau}\,\underline{\underline{B}}\cdot\underline{N}+T\underline{\underline{\psi}}\cdot\underline{\underline{B}}_{\underline{\xi}}\cdot\underline{N}+T\underline{\underline{\nu}}\cdot\underline{\underline{B}}^T\right] \tag{25}$$

$$\frac{d\underline{\tau}}{dz}=\frac{R_p}{\kappa}\underline{\lambda} \tag{26}$$

$$\frac{d\underline{\underline{\nu}}}{dz}=\begin{cases}-R_p\underline{\underline{\psi}}\cdot\underline{\underline{r}}_{\underline{\xi}}\cdot\underline{\alpha}+\frac{a-1}{1-z}\underline{\underline{\nu}} & z\neq 1\\ -\frac{1}{a}R_p\underline{\underline{\psi}}\cdot\underline{\underline{r}}_{\underline{\xi}}\cdot\underline{\alpha} & z=1\end{cases} \tag{27}$$

$$\frac{d\underline{\lambda}}{dz}=\begin{cases}-\left[\frac{d\underline{T}}{dz}\underline{\nu}\cdot\underline{C}_p+\frac{d\underline{\tau}}{dz}\underline{N}\cdot\underline{C}_p\right]+R_p\underline{\underline{\psi}}\cdot\underline{\underline{r}}_{\underline{\xi}}\cdot\Delta\underline{H}+\frac{a-1}{1-z}\underline{\lambda} & z\neq 1\\ \frac{1}{a}R_p\underline{\underline{\psi}}\cdot\underline{\underline{r}}_{\underline{\xi}}\cdot\Delta\underline{H} & z=1\end{cases} \tag{28}$$

with boundary conditions

$$\begin{array}{ll}\underline{\underline{\pi}}=0, & \underline{\tau}=0 \quad z=0\\ \underline{\underline{\nu}}=\underline{\underline{I}}, & \underline{\lambda}=\underline{e}_{\text{Nc}+1} \quad z=1\end{array} \tag{29}$$

Note that juxtaposition (e.g., $\underline{\tau}\,\underline{\underline{B}}$) denote tensor product, whereas the dot ($\underline{\underline{B}}\cdot\underline{N}$) denotes inner product. The gradients of $\underline{\underline{B}}$ in Eq. 25 and $\underline{r}$ in Eqs. 27 and 28 are calculated numerically.

Integrating Eqs. 25–28 together with 6–9 throughout the catalyst pellet by means of a fourth-order Runge-Kutta routine, $\underline{F}$, $\underline{G}$, $\underline{H}$, and $\underline{\underline{H}}_{\theta}$ are obtained for $z=1$, and thus Eq. 24 can be computed. In particular $\underline{\underline{H}}_{\theta}=\left[\underline{\underline{\nu}}\quad\underline{\lambda}\right]^T|_{z=1}$.

Homotopy continuation algorithm

The algorithm traces the solution branch of Eq. 21. The steps of the algorithm are as follows:

Table 2. Reference Conditions at the Catalyst Surface

T (K)	413
p_{CO} (Pa)	2431.8
p_{O_2} (Pa)	2431.8
p_{CO_2} (Pa)	0
p_{N_2} (Pa)	96461.4

Step 0. Initialization: Select initial values $\underline{X}_0 = \begin{bmatrix} \underline{\theta}_0 \\ 0 \end{bmatrix}$, and initial tangent vector $\dot{\underline{X}}_0 = \begin{bmatrix} \dot{\underline{\theta}}_0 \\ \dot{t}_0 \end{bmatrix}$, and a length step Δs. Set iteration counter $u = 1$.

Step 1. Solve $\underline{\varepsilon}(\underline{X}) = 0$ with the Newton's method, $\underline{X}_u^{(r+1)} = \underline{X}_u^{(r)} - \underline{\underline{\varepsilon}}_X^{-1}\left(\underline{X}_u^{(r)}\right) \cdot \underline{\varepsilon}\left(\underline{X}_u^{(r)}\right)$ using the initial point $\underline{X}_u^{(0)} = \underline{X}_{u-1} + \dot{\underline{X}}_{u-1}\Delta s$. Call $\underline{X}_u$ the solution found.

Step 2. Calculate the next tangent vector $\dot{\underline{X}}_u$ from $\underline{\underline{\varepsilon}}_X(\underline{X}_u) \cdot \dot{\underline{X}}_u = \begin{bmatrix} 0 \\ 1 \end{bmatrix}$ then scale it to take unit length.

Step 3. If all the desired solutions at $t = 1$ have been found, stop. Otherwise, set $u = u + 1$ and go to step 1.

This method is implemented in Matlab®, taking advantages of its user-friendly matrix manipulation.

Remarks

- If $\underline{\underline{\varepsilon}}_X$ is nonsingular and Δs is small enough, convergence of Newton is assured.
- $\underline{\underline{\varepsilon}}_X$ is singular in branching points. In such a case, it is desired to follow the two branches emanating from the branching point. Doedel[35] shows how to calculate these branches. However, branching does not occur in this problem.
- The algorithm has step controls on Δs to prevent divergence in Newton's method where the curvature is large and to increase the speed of the algorithm when the curvature is small.

It should be pointed out that the proposed algorithm finds all solutions of Eqs. 1–4 for a fixed Rp. All the physical solutions are found at $t = 1$, and the desired profiles are straightforwardly obtained.

Continuation algorithms implemented in tools such as AUTO[36] or MatCont[37] can be used to perform the continuation in Eq. 11, using Rp (or other physical parameter) as continuation parameter. However, good initial values of $(\underline{\theta}, R_p)$ should be provided to find the first solution of Eq. 11.

Furthermore, if only solutions for specific values of operating conditions are searched, it seems more advantageous using Eq. 13, as it is almost independent of the initial point.

The methodology proposed here always starts with a point in the solution curve of Eq. 13. The drawback, as it is shown in the following section, is that for certain initial points the curve does not pass for all physical solutions in $t = 1$. However, Kuno and Seader[19] give some criteria for choosing $\underline{X}_0$ so that all solutions belong to the curve $\underline{H} = 0$.

Results and Discussion

Experimental results in Table 1 showed that the rate of reaction increased for increasing pellet sizes. As in this case the value of thermal conductivity was large enough to handle the heat flux evolved, temperature can be considered constant in the range of pellet sizes analyzed (this assumption was confirmed in the simulations). This induces to think that the source of nonmonotonicity comes from the concentration. Thus, the rate expression used in this work is taken from Carberry,[38]

$$r = \frac{k\, p_{CO}}{(1 + K_{CO} p_{CO})^2} \tag{30}$$

whose shape is shown in Figure 1.

Table 3. Kinetic Parameters at 413 K

k (mol/Pa·m^3·s)	691.24
K_{CO} (1/Pa)	5.03×10^{-2}

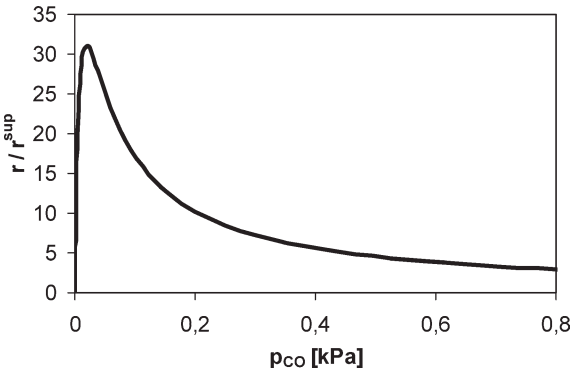

Figure 1. Dependence of the rate of reaction w.r.t. CO partial pressure.

Although in the CO oxidation reaction it is usual to use a Mars–van Krevelen-type kinetics, recently Vannice[39] has criticized its use, suggesting in turn a Langmuir–Hinshelwood-type kinetics like that in Eq. 30.

As the homotopy curves have intermediate solutions that do not have physical meaning, negative p_{CO} may occur. Thus, the denominator of Eq. 30 may become zero in the algorithm. To avoid division by zero, the expression

$$r = \frac{k\, p_{CO}}{(1 + K_{CO}|p_{CO}|)^2} \tag{31}$$

is used instead of Eq. 30.

Reference conditions at the catalyst surface and kinetic parameters are listed in Tables 2 and 3.

Parameter sensitivity

The sharp nonmonotonic dependence of r w.r.t. CO introduces a strong sensitivity, as shown in Figure 1.

Numerical problems arise when CO is near depletion, where the maximum of r occurs. Therefore, this kind of sensitivity shall be expected when conversion is high.

Homotopy curves

Homotopy curves are constructed departing from an initial value of $\underline{\theta}$. As curves can be tracked for both negative and positive values of t, the sign of $\dot{t}_0$ must be chosen positive so as to track the curve in the direction of interest. The initial predicting direction was chosen $\dot{\underline{X}}_0 = [\underline{0}\ 1]$.

The method used in this work obtains every possible steady state, that is, the state vector which drives Eq. 11 to

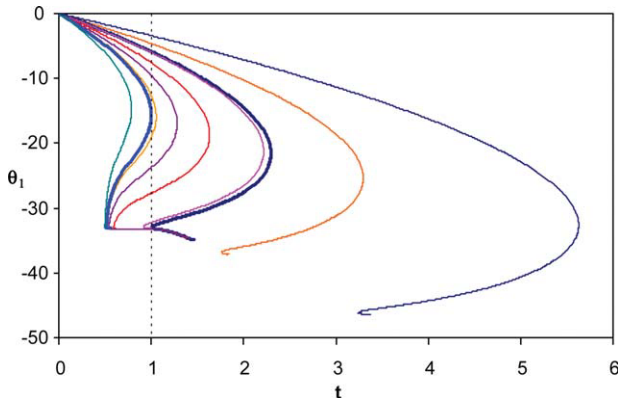

Figure 2. Homotopy curves for different pellet sizes.

[Color figure can be viewed in the online issue, which is available at wileyonlinelibrary.com.]

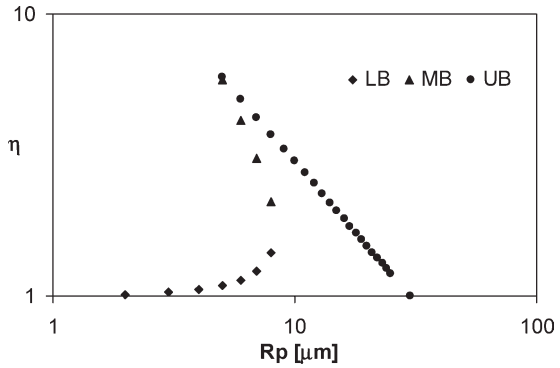

Figure 3. Effectiveness factor vs. pellet size.

zero for different values of Rp. The only points of these curves, which have a physical meaning are those obtained for $t = 1$, as in this case $\underline{H} = 0$ becomes $\underline{F} = 0$, which is the original problem. Thus, the homotopy method presented in this work must be run for different values of Rp, each time obtaining all available solutions for $t = 1$. Appendix B shows a validation of the method proposed in this work.

Figure 2 illustrates homotopy curves for different pellet sizes. The thicker lines correspond to the limits of the multiplicity region, i.e. the curves that cross $t = 1$ more than once.

When $t = 1$, θ_1 is the molar flux of CO at the surface, value with which the effectiveness factor is computed by virtue of Eq. 10 and plotted in Figure 3.

This curve shows three regions: lower, middle, and upper branches. Moreover, Figure 3 shows that in the region between $Rp = 5$ and $Rp = 8$ μm (approximately), the three branches coexist and multiplicity takes place.

It can be seen in the upper branch in Figure 3 that η depends inversely upon Rp. On the other hand, Figure 2 shows that the solution corresponding to the upper branch has the same value for different Rp. Analyzing Eq. 10, for constant surface temperature and reactants composition the expression $\frac{N_j^{sup}}{r_j^{sup}}$ is constant, thus obtaining a constant value of the molar flux of any species at the surface, regardless of the pellet size. Therefore, the effectiveness factor is inversely proportional to Rp, in accordance to the asymptotic behavior when the catalyst operates at diffusive control (large values of Thiele modulus).

Dependence on initial conditions

Figure 4 shows typical curves θ_1 vs. t when (a) $Rp = 2$ μm, (b) $Rp = 7$ μm, and (c) $Rp = 12$ μm, for different initial values of θ_1 and constant initial value of θ_2.

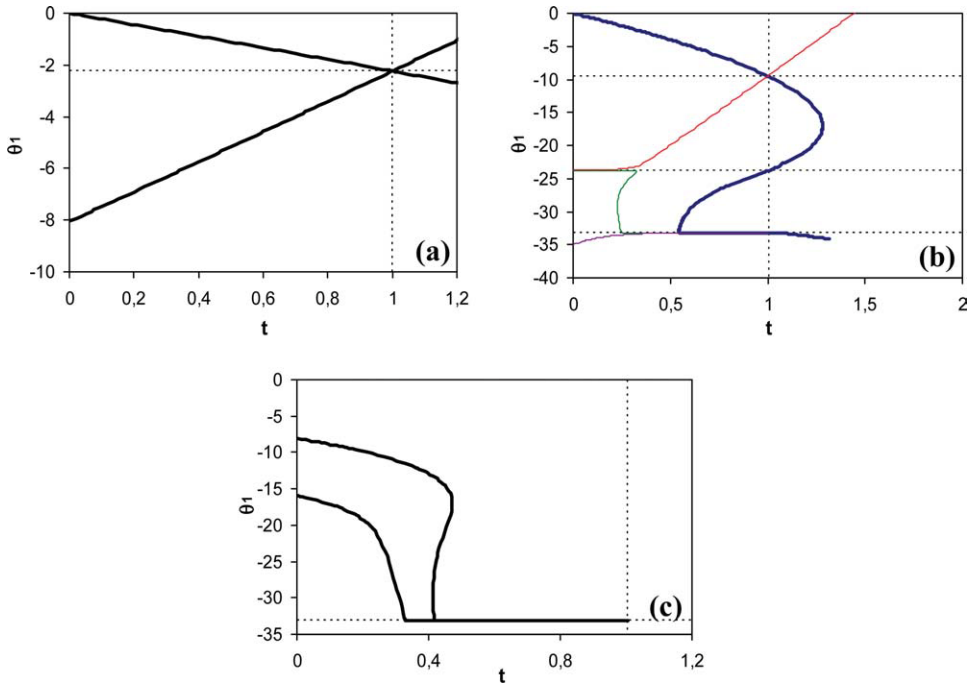

Figure 4. Homotopy curves for different initial values of θ_1 for (a) $R_p = 2$ μm, (b) $R_p = 7$ μm, (c) $R_p = 12$ μm.

[Color figure can be viewed in the online issue, which is available at wileyonlinelibrary.com.]

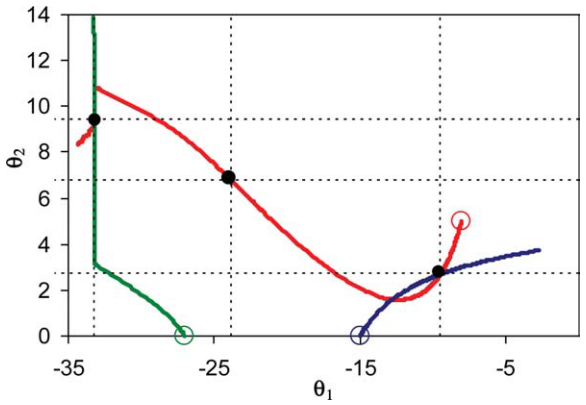

Figure 5. Curves $\underline{H}(\underline{\theta};t)=\underline{0}$ for R_p = 7 μm in (θ_1, θ_2)-space.

[Color figure can be viewed in the online issue, which is available at wileyonlinelibrary.com.]

Figure 4a shows the typical behavior for small pellet sizes of any homotopy curve to reach the single steady state condition. The solution for this case is readily obtained. On the other hand, Figure 4b shows the dependence of the method on the initial value of θ_1 to find the multiple steady states. It can be seen that initial values of θ_1 above c. -9.5 (the upper steady state) allow the curve to find the three steady states. Any value within -9.5 and -23.8 (the middle steady state) allows the curve to find only the first steady state. Within the range of -23.8 to -33.2 (the lower steady state), the curve passes only through the third steady state. For initial values of θ_1 lower than -33.2, numerical problems arise, although values lower but sufficiently close to -33.2 show that only the lower steady state is reached.

Figure 4b also suggests that when starting from a value in the neighborhood of the middle steady state, this steady state, which is known to be physically unstable,[1] cannot be easily reached by the method unless a very accurate value is adopted, as small perturbations from the exact value lead to either the first or the third steady states.

Figure 4c shows the typical behavior of the zero-curve for large pellet sizes. It must be said that the algorithm cannot always trace the zero-curve for *Rp* greater than about 8 μm up to $t = 1$. Numerical difficulties arise when integrating in condition of total depletion inside the pellet. When this case occurs, step controls must be applied, and thus the algorithm becomes slower in traversing this zone.

The dependence of the number of steady states achievable upon the initial $\underline{\theta}$, shown in Figure 4b, agrees with the result of Kuno and Seader[19] for whom $\underline{\theta}_0$ should be selected such that $\underline{F}(\underline{\theta})-\underline{\theta}+\underline{\theta}_0=\underline{0}$ has a minimum number of solutions. Since $\underline{F}(\underline{\theta})$ is assumed to be bounded in the domain of interest, extreme values of $\underline{\theta}_0$ should satisfy the condition.

Figure 5 depicts the homotopy curves in the (θ_1,θ_2)-space. Initial values $\underline{\theta}_0$ are shown with hollow circles and steady states with solid circles. It can be seen that only initial values in the region of $\theta_1 > -9.5$ (regardless of the value of θ_2) reach the three steady states, as already mentioned.

As regards θ_2, when $t = 1$ it represents the heat flux at the surface. It was observed that temperature remained constant throughout the pellet. Therefore, the system is rather insensitive to heat flux, so initial conditions of θ_2 are not critical. This was verified by numerical results not shown. If the thermal conductivity was such that temperature gradients existed, initial values of θ_2 may have analogous impact as θ_1.

Conclusions

In this work, an algorithm that allows finding multiple steady states in a catalyst pellet with a nonmonotonic kinetics is presented. The equation system that arises when simulating the pellet is highly nonlinear and traditional solver packages fail either to converge or to find all possible steady states. The method proposed in this work, based on homotopy continuation, finds every steady state by tracking a curve from a fairly arbitrary initial point.

A sensitivity study of the homotopy curves w.r.t. $\underline{\theta}_0$ was performed. Although homotopy curves can be tracked from any starting point, it was observed that there is a region of θ_1 for which curves pass through the three solutions and other regions departing from which only one of the three solutions is achieved. The limits of these regions are determined by the values of θ_1 in the three solutions. These regions are independent of the initial value of θ_2 (which represents the heat flux) as the thermal conductivity is high enough to guarantee constant temperature within the pellet.

Numerical instabilities occur around the total depletion of the reactant, where the kinetics is strongly sensitive to this reactant composition. This happens for the solutions in the upper branch in Figure 3. In some cases, this difficulty is overcome applying step controls, but yet when the problem persists, an asymptotic behavior of the curve is observed, tending to the correct solution.

Even when in practice pellet sizes to be used are far from the multiplicity region, experimental data to fit kinetic parameters fall in this range of multiplicity. Thus, it is important to take this effect into account when analyzing the experimental data.

This study also suggests that the kinetics of a reaction that produces in a certain range increasing effectiveness factors for increasing pellet sizes should behave nonmonotonically, when no thermal effects are present. This would discard a Mars–van Krevelen type kinetics for the CO oxidation reaction catalyzed by copper/ceria catalysts.

Acknowledgments

Authors wish to thank Universidad de Buenos Aires, ANPCyT, and CONICET for their financial support.

Notation

a = shape factor
$\underline{\underline{B}}$ = dusty gas model matrix [s/m^2]
$\underline{\underline{Cp}}$ = species heat capacities [J/mol·K]
$\underline{e}$ = basis vector
$\underline{F}$ = system of equations of the real problem
$\underline{G}$ = system of equations for the "easy" problem
$\underline{H}$ = homotopy function
$\Delta\underline{H}$ = reaction enthalpies [J/mol]
$\underline{\underline{I}}$ = identity matrix
$\bar{k}$ = kinetic constant [mol/m^3·s·Pa]
K_{CO} = adsorption constant of CO [1/Pa]
$\underline{N}$ = species molar fluxes [mol/m^2·s]
Nc = number of species
Nn = system dimension
Nu = Nusselt number

$\underline{p}$ = species partial pressure [Pa]
$\underline{q}$ = heat flux [J/m^2·s]
$\underline{r}$ = reaction rates [mol/m^3·s·Pa]
R = universal constant of gases [J/mol·K]
R_p = pellet size [μm]
s = arclength
Sh = Sherwood number
t = homotopy parameter
T = temperature [K]
$\underline{X}$ = points of the homotopy curve
z = dimensionless space coordinate

Greek letters

$\underline{\underline{\alpha}}$ = stoichiometric coefficients
$\underline{\underline{\delta}}$ = Kronecker Delta
$\underline{\underline{\varepsilon}}_X$ = Jacobian matrix of the augmented system
φ = additional equation for the augmented system
η = effectiveness factor
$\underline{\theta}$ = homtopy variables
κ = thermal conductivity of the solid [J/m·K·s]
$\underline{\lambda}$ = gradient of q w.r.t. θ
$\underline{\nu}$ = gradient of $\underline{N}$ w.r.t. θ
$\underline{\xi}$ = state variables (partial pressures and temperature)
$\underline{\underline{\pi}}$ = gradient of $\underline{p}$ w.r.t. θ
$\underline{\tau}$ = gradient of T w.r.t. θ
$\underline{\underline{\psi}}$ = gradient of $\underline{\xi}$ w.r.t. θ

Subscripts and superscripts

0 = starting value
j,k = species j, k
i = reaction i
n = element n of vector $\underline{\theta}$
(r) = iteration r
sup = surface
T = transpose
u = point u on the zero-curve

Literature Cited

1. Elnashaie S, Elshishini S. *Modelling, simulation and optimization of industrial fixed bed catalytic reactors*. Amsterdam: Gordon and Breach Science Publishers, 1993.
2. Bilous O, Amundson NR. Chemical reactor stability and sensitivity. *AIChE J*. 1955;1:513–521.
3. Aris R, Amundson NR. An analysis of chemical reactor stability and control-I: the possibility of local control, with perfect or imperfect control mechanisms. *Chem Eng Sci*. 1958;7:121–131.
4. Aris R, Amundson NR. An analysis of chemical reactor stability and control-II: the evolution of proportional control. *Chem Eng Sci*. 1958; 7:132–147.
5. Aris R, Amundson NR. An analysis of chemical reactor stability and control-III: the principles of programming reactor calculations. *Some extensions*. *Chem Eng Sci*. 1958;7:148–155.
6. Jorgensen D, Farr W, Aris R. More on the dynamics of a stirred tank with consecutive reactions. *Chem Eng Sci*. 1984;39:1741–1752.
7. Balakotaiah V, Luss D. Multiplicity features of reacting systems: dependence of the steady-states of a CSTR on the residence time. *Chem Eng Sci*. 1983;38:1709–1721.
8. Lee C, Morbidelli M, Varma A. Steady state multiplicity behavior of an isothermal axial dispersion fixed-bed reactor with nonuniformly active catalyst. *Chem Eng Sci*. 1987;42:1595–1608.
9. Weisz PB, Hicks JS. The behaviour of porous catalyst particles in view of internal mass and heat diffusion effects. *Chem Eng Sci*. 1962;17:265–275.
10. Amundson N, Raymond LR. Stability in distributed parameter systems. *AIChE J*. 1965;11:339–350.
11. Van den Bosch B, Luss D. Uniqueness and multiplicity criteria for an nth order chemical reaction. *Chem Eng Sci*. 1977;32:203–212.
12. Hu R, Balakotaiah V, Luss D. Multiplicity features of porous catalytic pellets-I. Single zeroth-order reaction case. *Chem Eng Sci*. 1985;40:589–598.
13. Hu R, Balakotaiah V, Luss D. Multiplicity features of porous catalytic pellets-II. Influence of reaction order and pellet geometry. *Chem Eng Sci*. 1985;40:599–610.
14. Nielsen P, Villadsen J. An analysis of the multiplicity pattern of models for simultaneous diffusion, chemical reaction and absorption. *Chem Eng Sci*. 1985;40:571–587.
15. Tsotsis T. Nonuniform steady states in systems of interacting catalyst particles: the case of negligible interparticle mass transfer coefficient. *Chem Eng Commun*. 1981;11:27–58.
16. Schmitz R, Tsotsis T. Spatially patterned states in systems of interacting catalyst particles. *Chem Eng Sci*. 1983;38:1431–1437.
17. Botero A, Garhyan P, Elnashaie S. Bifurcation and chaotic behaviour of a coupled acetylcholinesterase/choline acetyltransferase difusion-reaction enzymes system. *Chem Eng Sci*. 2004;59:581–597.
18. Giunta P, Bergamini M, Moreno M, Mariño F, Laborde M, Amadeo N. Multiplicidad de estados estacionarios en una pastilla catalítica isotérmica. Proceedings of XVI Congreso Argentino de Catálisis, Buenos Aires, August 2009.
19. Kuno M, Seader J. Computing all real solutions to systems of nonlinear equations with a global fixed-point homotopy. *Ind Eng Chem Res*. 1988;27:1320–1329.
20. Gritton K, Seader J, Lin W. Global homotopy procedures for seeking all roots of a nonlinear equation. *Comp Chem Eng*. 2006; 25:1003–1019.
21. Davidenko DF. On the approximate solution of systems of non-linear equations. *Ukrain Mat Zh*. 1953;5:196–206.
22. Keller H. *Numerical solution of bifurcation and nonlinear eigenvalue problems*. In: Rabinowitz PH, editor. *Applications of Bifurcation Theory*. Ciudad: Academic Press, 1977:359–384.
23. Watson LT. A globally convergent algorithm for computing fixed points of C^2 maps. *Appl Math Comput*. 1979;5:297–311.
24. Watson LT. Numerical linear algebra aspects of globally convergent homotopy methods. *SIAM Rev*. 1986;28:529–545.
25. García C, Zangwill W. Determining all solutions to certain systems of nonlinear equations. *Math Oper Res*. 1979;4:1–14.
26. Allgower EL, Georg K. *Numerical path following*. In: Ciarlet PG and Lions JL, editor, *Handbook of Numerical Analysis*. Amsterdam: North Holland, 1997:3–207.
27. Krishna R. A simplified procedure for the solution of the Dusty Gas Model equations for steady—state transport in nonreacting systems. *Chem Eng J*. 1987;35:75–81.
28. Krishna R, Standart G. Mass and energy transfer in multicomponent systems. *Chem Eng Commun*. 1979;3:201–275.
29. Laborde M, Amadeo N, Giunta P. Hydrogen production from ethanol steam reforming. Fixed bed reactor design. *Int J Chem Reactor Eng*. 2008;6:A12. Available at: http://www.bepress.com/ijcre/vol6/A12.
30. Krishna R, Wesselingh J. The Maxwell–Stefan approach to mass transfer. *Chem Eng Sci*. 1996;52:861–911.
31. Watson LT. An algorithm that is globally convergent with probability one for a class of nonlinear two-point boundary value problems. *SIAM J Numer Anal*. 1979;16:394–401.
32. Hlavacek M, Kubicek V. *Numerical Solutions of Non-Linear Boundary Value Problems With Applications*. Englewood Cliffs, NJ: Prentice Hall, 1983.
33. Rheinboldt W. Numerical methods for a class of finite dimensional bifurcation problems. *SIAM J Numer Anal*. 1978;15:1–11.
34. Keller HB. *Lectures on Numerical Methods in Bifurcation Problems*. Berlin: Springer Verlag, 1987.
35. Doedel EJ. *Lecture Notes on Numerical Analysis of Nonlinear Equations*. Montreal: Concordia University, 2005. Available at: http://cmvl.cs.concordia.ca/courses/comp-6361/fall-2005/.
36. Doedel EJ, Champneys AR, Fairgrieve TF, Kuznetsov YA, Sandstede B, Wang XJ. *AUTO97: Continuation and Bifurcation Software for Ordinary Differential Equations (with Hom-Cont). User's Guide*. Concordia University: Montreal, Canada, 1997.
37. Dhooge A, Govaerts W, Kuznetsov YA. *Matcont: A Matlab Package For Numerical Bifurcation Analysis of Odes*. Dept. of Applied Mathematics and Computer Science: Krijgslaan 281-S9, 9000 Ghent, Belgium.
38. Carberry J. Ingeniería de Las Reacciones Químicas y Catalíticas. Editorial. Géminis, Buenos Aires, 1980.
39. Vannice A. An analysis of the Mars-van Krevelen rate expression. *Cat Today*. 2007;123:18–22.

40. Giunta P, Amadeo N, Laborde M. Simulation of a low temperature water gas shift reactor using the heterogeneous model/application to a PEM fuel cell. *J Power Sources*. 2006;156:489–496.

Appendix A: Auxiliary Differential Equations

As $\underline{\underline{H}}_\theta = t\underline{\underline{F}}_\theta + (1-t)\underline{\underline{G}}_\theta$ and $\underline{\underline{G}}_\theta$ is a diagonal matrix with the scale factor in its diagonal, all the effort is focused on $\underline{\underline{F}}_\theta$. As regards t, it is constant for the integration in z. It can also be said that θ_n are also independent from z. Thus, Eqs. 1–4 can be used in the following form[40]

$$\frac{\partial}{\partial\theta_n}\left(\frac{dp_j}{dz}\right) = \frac{d}{dz}\left(\frac{\partial p_j}{\partial\theta_n}\right) = \frac{d\pi_{nj}}{dz} = R_p R\frac{\partial}{\partial\theta_n}(T\,B_{jk}N_k) \quad \text{(A.1)}$$

Analogously

$$\frac{d\tau_n}{dz} = \frac{R_p}{\kappa}\frac{\partial q}{\partial\theta_n} \quad \text{(A.2)}$$

$$\frac{dv_{nj}}{dz} = \begin{cases} -R_p\alpha_{ij}\frac{\partial r_i}{\partial\theta_n} + \frac{a-1}{1-z}\frac{\partial N_j}{\partial\theta_n} & z \neq 1 \\ -\frac{1}{a}R_p\alpha_{ij}\frac{\partial r_i}{\partial\theta_n} & z = 1 \end{cases} \quad \text{(A.3)}$$

$$\frac{d\lambda_n}{dz} = \begin{cases} -C_{p_j}N_j\frac{d}{dz}\frac{\partial T}{\partial\theta_n} + R_p\Delta H_i\frac{\partial r_i}{\partial\theta_n} + \frac{a-1}{1-z}\frac{\partial q}{\partial\theta_n} & z \neq 1 \\ -\frac{1}{a}R_p\Delta H_i\frac{\partial r_i}{\partial\theta_n} & z = 1 \end{cases} \quad \text{(A.4)}$$

where repeated indexed indicate summation. In the same way, boundary conditions[5] are transformed into

$$\begin{array}{ll} \frac{\partial p_j}{\partial\theta_n} = 0, \frac{\partial T}{\partial\theta_n} = 0 & z = 0 \\ \frac{\partial N_j}{\partial\theta_n} = \delta_{nj}, \frac{\partial q}{\partial\theta_n} = \delta_{nNc+1} & z = 1 \end{array} \quad \text{(A.5)}$$

where δ is the Kronecker delta.

Equations A.1–A.4 can be rewritten with these new variables introduced in tensorial form by means of adding bases and dot and tensorial products.

$$\frac{d\pi_{nj}}{dz}\underline{e}_n\underline{e}_j = R_p R\Big[\tau_n\underline{e}_n B_{jk}\underline{e}_j\underline{e}_k\cdot N_l\underline{e}_l + T\frac{\partial\xi^r}{\partial\theta_n}\underline{e}_n\underline{e}_r\cdot\frac{\partial B_{jk}}{\partial\xi^s}\underline{e}_s\underline{e}_j\underline{e}_k \times N_l\underline{e}_l + Tv_{nl}\underline{e}_n\underline{e}_l\cdot B_{jk}\underline{e}_k\underline{e}_j$$

$$\frac{d\tau_n}{dz}\underline{e} = \frac{R_p}{\kappa}\lambda_n\underline{e}_n$$

$$\frac{dv_{nj}}{dz}\underline{e}_n\underline{e}_j = \begin{cases} -R_p\frac{\partial\xi^r}{\partial\theta_n}\underline{e}_n\underline{e}_r\cdot\frac{\partial r_i}{\partial\xi^s}\underline{e}_s\underline{e}_i\cdot\alpha_{ij}\underline{e}_i\underline{e}_j + \frac{a-1}{1-z}v_{nj}\underline{e}_n\underline{e}_j & z \neq 1 \\ -\frac{1}{a}R_p\frac{\partial\xi^r}{\partial\theta_n}\underline{e}_n\underline{e}_r\cdot\frac{\partial r_i}{\partial\xi^s}\underline{e}_s\underline{e}_i\cdot\alpha_{ij}\underline{e}_i\underline{e}_j & z = 1 \end{cases}$$

$$\frac{d\lambda_n}{dz}\underline{e}_n = \begin{cases} -\left[\frac{dT}{dz}v_{nj}\underline{e}_n\underline{e}_j + \frac{d\tau_n}{dz}\underline{e}_n N_j\underline{e}_j\right]\cdot Cp_k\underline{e}_k + \\ R_p\frac{\partial\xi^r}{\partial\theta_n}\underline{e}_n\underline{e}_r\cdot\frac{\partial r_i}{\partial\xi^s}\underline{e}_s\underline{e}_i\cdot\Delta H_m\underline{e}_m + \frac{a-1}{1-z}\lambda_n\underline{e}_n & z \neq 1 \\ \frac{1}{a}R_p\frac{\partial\xi^r}{\partial\theta_n}\underline{e}_n\underline{e}_r\cdot\frac{\partial r_i}{\partial\xi^s}\underline{e}_s\underline{e}_i\cdot\Delta H_m\underline{e}_m & z = 1 \end{cases}$$

These lead to

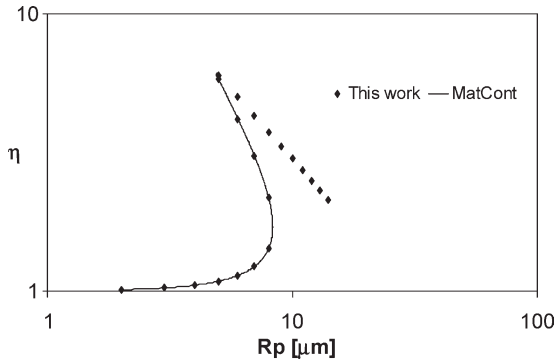

Figure A1. Comparison of the two methods.

$$\frac{d\underline{\underline{\pi}}}{dz} = R_p R\left[\underline{\tau}\underline{B}\cdot\underline{N} + T\underline{\psi}\cdot\underline{\underline{B}}_{\underline{\xi}}\cdot\underline{N} + T\underline{v}\cdot\underline{\underline{B}}^T\right] \quad \text{(A.6)}$$

$$\frac{d\underline{\tau}}{dz} = \frac{R_p}{\kappa}\underline{\lambda} \quad \text{(A.7)}$$

$$\frac{d\underline{\underline{v}}}{dz} = \begin{cases} -R_p\underline{\psi}\cdot\underline{r}_{\underline{\xi}}\cdot\underline{\underline{\alpha}} + \frac{a-1}{1-z}\underline{\underline{v}} & z \neq 1 \\ -\frac{1}{a}R_p\underline{\psi}\cdot\underline{r}_{\underline{\xi}}\cdot\underline{\underline{\alpha}} & z = 1 \end{cases} \quad \text{(A.8)}$$

$$\frac{d\underline{\lambda}}{dz} = \begin{cases} -\left[\underline{v}\frac{dT}{dz} + \frac{d\underline{\tau}}{dz}\underline{N}\right]\cdot\underline{C}_p + R_p\underline{\underline{\psi}}\cdot\underline{r}_{\underline{\xi}}\cdot\Delta\underline{H} + \frac{a-1}{1-z}\underline{\lambda} & z \neq 1 \\ \frac{1}{a}Rp\ \underline{\psi}\cdot\underline{r}_{\underline{\xi}}\cdot\Delta\underline{H} & z = 1 \end{cases} \quad \text{(A.9)}$$

Appendix B: Model Validation

The package MatCont[37] was used to validate the method presented in this work. This package is coded in Matlab® as well as the algorithm used in this work. MatCont allows performing the continuation in Rp departing from a good initial point. It may calculate the Jacobian in Eq. 16 either analytically if the expression is available (which is not the case) or numerically running the integration of the system from $z = 0$ to $z = 1$, $(Nn + 1)$ times to compute all of the partial derivatives required, whereas the algorithm presented in this work computes the Jacobian integrating only once, although more equations need to be integrated.

In both MatCont and the method presented in this work, numerical difficulties arise when integrating in condition of total depletion inside the pellet. MatCont could not trace the curve beyond $Rp = 5$ μm in the upper branch, either because an error occurs or the successive solutions do not follow a smooth curve. This takes place for solutions with high CO fluxes.

Effectiveness factors for different Rp obtained by both methods are shown in Figure A1.

Figure A1 shows that both methods agree in the results.

Manuscript received July 23, 2009, and revision received Mar. 9, 2010.